Redox Biology 84 (2025) 103657

Contents lists available at ScienceDirect

Redox Biology

journal homepage: www.elsevier.com/locate/redox

Ferroptosis in acute liver Failure: Unraveling the hepcidin-ferroportin axis and therapeutic interventions

Jinyong He [a,b,c,1], Cong Du [a,b,c,**,1], Cuiping Li [a,b,1], Wei Li [a,b,c], Jinlan Qiu [a,b,c], Mingpeng Ma [a,b,c], Yunhao Chen [b], Qi Zhang [a,b,c,*]

[a] Cell-gene Therapy Translational Medicine Research Center, The Third Affiliated Hospital, Sun Yat-sen University, Guangzhou, Guangdong, China
[b] Biotherapy Center, The Third Affiliated Hospital, Sun Yat-sen University, Guangzhou, Guangdong, China
[c] Guangdong Province Key Laboratory of Liver Disease Research, The Third Affiliated Hospital, Sun Yat-sen University, Guangzhou, Guangdong, China

ARTICLE INFO

Keywords:
Acute liver failure
Mesenchymal stromal cells
Ferroptosis
Iron metabolism
Hepcidin-ferroportin axis

ABSTRACT

Acute liver failure (ALF) represents a critical clinical syndrome marked by massive hepatocyte death and severe functional deterioration. While metabolic dysregulation is a recognized hallmark, the pathophysiological implications of iron metabolism disturbance in ALF progression remain poorly understood, which may unveil novel therapeutic targets. Using clinical samples and preclinical murine models, we identified ferroptosis as a predominant pathological feature in ALF-affected livers. Notably, pharmacological inhibition of ferroptosis significantly attenuated disease progression in experimental ALF. Mechanistically, dysregulation of the hepcidin-ferroportin (FPN) axis drives hepatic iron overload, precipitating ferroptotic cell death in ALF. The anti-rheumatoid arthritis drug auranofin restored hepcidin-FPN axis homeostasis and mitigated liver injury, though concomitant upregulation of proinflammatory cytokines limited its therapeutic potential. Strikingly, mesenchymal stromal cells (MSCs) demonstrated superior therapeutic efficacy, coordinately modulating the hepcidin-FPN axis while suppressing ferroptosis through PI3K/Akt/Nrf2 pathway activation. Our findings not only establish the causal relationship between hepcidin-FPN axis dysfunction and ferroptosis-driven liver injury, but also propose MSC-based therapy as a multifaceted strategy targeting both iron homeostasis and ferroptosis for ALF management.

1. Introduction

Acute liver failure (ALF) is a refractory, life-threatening liver disease characterized by the abrupt loss of a substantial number of hepatocytes and catastrophic impairment of liver function. As an end-stage condition, liver transplantation remains the sole definitive treatment for ALF [1,2]. However, this approach is significantly constrained by the critical shortage of donated liver grafts. The short-term mortality rate of ALF exceeds one-third in the absence of timely liver transplantation [3,4]. ALF not only threatens patients' health and lives but also severely disrupts their occupational and social roles, placing immense pressure on both families and societies [5]. Hence, it is imperative to elucidate the underlying mechanisms of ALF and develop innovative therapeutic strategies.

The abrupt death of massive hepatocytes constitutes a pivotal event in triggering the progression of ALF. In recent years, various patterns of cell death have been identified [6–11]. Ferroptosis, an iron-dependent and regulated form of cell death discovered in the past decade [12–14]. Previous researches have demonstrated that ferroptosis plays a key role in ALF, predominantly through mechanisms involving lipid peroxidation and oxidative stress [8,11,15–18]. It should be noted that intracellular iron accumulation establishes the critical conditions necessary for lipid peroxidation and promotes its progression [12,14]. To fully illustrate the comprehensive landscape of ALF from the viewpoint of ferroptosis, it is crucial to delve deeper into the regulatory mechanisms of iron metabolism and explore potential intervention strategies that target these processes.

The liver serves as the central regulator of iron metabolism and maintains systemic iron homeostasis through diverse mechanisms [19,

* Corresponding author. Biotherapy Center, The Third Affiliated Hospital, Sun Yat-sen University, Guangzhou, Guangdong, 510630, China.
** Corresponding author. Biotherapy Center, The Third Affiliated Hospital, Sun Yat-sen University, Guangzhou, Guangdong, 510630, China.
E-mail addresses: ducong3@mail.sysu.edu.cn (C. Du), zhangq27@mail.sysu.edu.cn (Q. Zhang).
[1] These authors contributed equally: Jinyong He, Cong Du and Cuiping Li.

https://doi.org/10.1016/j.redox.2025.103657
Received 11 February 2025; Received in revised form 10 April 2025; Accepted 30 April 2025
Available online 8 May 2025

Abbreviations

ALF	acute liver failure
TAA	thioacetamide
MSCs	mesenchymal stromal cells
FPN	ferroportin
TBI	transferrin-bound iron
TFR1	transferrin receptor 1
NTBI	non-transferrin-bound iron
SLC39A14	solute carrier family 39 member 14
IBA1	Ionized Calcium-Binding Adapter Molecule 1
HCs	healthy controls
PCA	principle component analysis
TEM	transmission electron microscopy
AST	aspartate aminotransferase
ALT	alanine aminotransferase
GSEA	gene set enrichment analysis
AUR	Auranofin
APAP	acetaminophen
Con A	concanavalin A
DEGs	differentially expressed genes
TFs	transcription factors
CCl4	carbon tetrachloride
Tfrc	Transferrin receptor
ROS	reactive oxygen species
GSH	glutathione
LPS	lipopolysaccharide
GalN	d-galactosamine.

20]. Imbalances of iron homeostasis can contribute to or exacerbate liver injury. Conversely, liver injury may also disrupt iron homeostasis, thereby establishing a vicious cycle [21,22]. Therefore, understanding how to regulate iron metabolism and maintain its homeostasis is pivotal for preventing and treating ALF. Regarding iron uptake and transport, hepatocytes are capable of internalizing iron bound to transferrin (TBI) through the transferrin receptor 1 (TFR1), as well as non-transferrin-bound iron (NTBI) via the solute carrier family 39 member 14 (SLC39A14) [19,20,23]. It is NTBI, a highly toxic form of iron, that serves as a primary biomarker of iron overload and causes oxidative damage [24]. Regarding iron storage and release, ferritin functions as the principal intracellular storage protein for iron, while ferroportin (FPN), the only known iron exporter in mammals, mediates its release when required. Notably, hepatocytes synthesize and secrete hepcidin, a key regulator of systemic iron homeostasis that precisely controls iron absorption and release. Specifically, hepcidin binds to ferroportin, triggering its degradation to regulate iron efflux and prevent toxic iron accumulation [25,26]. In alcoholic liver disease [22], chronic viral hepatitis [27] and liver fibrosis [28], the abnormal expression of hepcidin or ferroportin impacts their pathophysiological processes. However, the precise role of the hepcidin-ferroportin axis in ALF and the potential intervention strategies remain to be elucidated.

Mesenchymal stromal cells (MSCs), also known as medicinal signaling cells, are present in various adult tissues such as umbilical cord, bone marrow, and adipose tissue [29]. MSCs have demonstrated considerable potential in treating liver diseases due to their remarkable paracrine effects, robust immunomodulatory properties, and tissue repair capabilities. [30–34]. Preclinical and preliminary clinical studies conducted by our group [35,36] and others [37–39] have demonstrated the efficacy and safety of MSCs, thereby highlighting their promising prospects for liver protection. However, the precise and comprehensive mechanisms underlying the therapeutic effects of MSCs in ALF remain incompletely elucidated, which somewhat hampers their extensive clinical application. In particular, the mechanism by which MSCs regulate iron metabolism remains poorly understood.

Our present research elucidates the crucial role of ferroptosis in ALF, where dysregulation of the hepcidin-ferroportin signal axis disrupts iron homeostasis and initiates subsequent hepatic ferroptosis. Interestingly, we found that Auranofin (AUR), an FDA-approved drug for rheumatoid arthritis, exhibited hepatoprotective effects through the upregulation of hepcidin expression in the liver. These findings underscore the significant involvement of the hepcidin-ferroportin axis in ALF progression. However, AUR concurrently induced the expression of pro-inflammatory cytokines. Furthermore, our study highlights that MSCs modulate the hepcidin-ferroportin axis through the PI3K/Akt/Nrf2 pathway, thereby finely regulating iron metabolism and effectively inhibiting ferroptosis, leading to enhanced therapeutic outcomes in ALF.

2. Materials and methods

2.1. Reagents

Thioacetamide (#163678) and DMSO (#472301) were purchased from Sigma-Aldrich (St. Louis, MO, USA). Deferoxamine mesylate (#S5742), RSL3 (#S8155), ML385 (#S8790), MK-2206 (#S1078), and corn oil (#S6701) were obtained from Selleck Chemicals (Houston, TX, USA). Liproxstatin-1 (#HY-12726), Auranofin (#HY-B1123), and PEG300 (#HY-Y0873) were purchased from MedChemExpress (MCE) (Shanghai, China). Tween 80 (#MB2675) and normal saline (#MA0083) were purchased from MeilunBio (Dalian, China).

2.2. Human samples

Our experiments with human liver samples were conducted in accordance with the research board protocol of the medical ethical committees of the Third Affiliated Hospital of Sun Yat-sen University. Informed consent was obtained from all subjects, and the experiment conforms to the principles set out in the WMA Declaration of Helsinki and the Department of Health and Human Services Belmont Report. Human liver tissues were acquired from nonviable grafts following liver transplantation procedures.

2.3. Animal experiments

All animal procedures were approved by the Experimental Animal Care Commission of the Third Affiliated Hospital of Sun Yat-sen University. Six-to eight-week-old male C57BL/6 mice (control mice (n = 6), ALF mice (n = 20), MSCs treated mice (n = 12), Lip-1 treated mice (n = 12), DFOM treated mice (n = 12), ML385 treated mice (n = 12), Auranofin treated mice (n = 12)) were randomly divided into groups. Mice were raised in a specific pathogen-free (SPF) environment with constant temperature (22 ± 1 °C) and relative humidity (50 ± 5 %), and had free access to food and water. Next, mice were intraperitoneally injected with a single dose of TAA (150 mg/kg, dissolved in sterile saline) or saline. Twelve hours later, for MSCs administration, 2×10^6 cells (hUC-MSCs) were suspended in 0.2 ml of saline and transplanted into mice via tail vein injection. DFOM (100 mg/kg, dissolved in sterile saline), Lip-1 (10 mg/kg, dissolved in 10 % DMSO + 40 % PEG300 + 5 % Tween-80 + 45 % sterile saline), ML385 (30 mg/kg, dissolved in 10 % DMSO + 40 % PEG300 + 5 % Tween-80 + 45 % sterile saline), and Auranofin (5 mg/kg, dissolved in 10 % DMSO + 90 % corn oil) were intraperitoneally injected into mice. The survival of all mice was recorded for 24 h, after which liver tissues were harvested for pathological analysis.

2.4. Serum biochemical Indexes detection

Liver enzymes, including aspartate aminotransferase (AST) and alanine aminotransferase (ALT), were examined using the Hitachi Automatic Analyzer (3100; Hitachi Ltd., Tokyo, Japan). Cytokines and chemokines in serum were measured and quantified using the Milliplex® mouse immunology panel (Merck, MHSTCMAG-70K) according to the manufacturer's instructions. Each experimental group comprised three mice.

2.5. Measurements of non-heme iron, non-transferrin-bound iron (NTBI), hepcidin and IL-6

Tissue iron content was quantified using a colorimetric assay kit (I291, Dojindo Laboratories) following the manufacturer's protocol. Serum and tissue levels of non-transferrin-bound iron (NTBI) were measured using an ELISA kit (MM-46281M1, MEIMIAN) following the protocol provided by the manufacturer. Tissue hepcidin concentrations were measured with a Hepcidin ELISA kit (MM-44770M1, MEIMIAN) as per the manufacturer's guidelines. Serum interleukin-6 (IL-6) levels were assessed using a mouse IL-6 ELISA kit (550950, BD) in accordance with the manufacturer's specifications. Each experimental group comprised three mice.

2.6. Perls' blue staining

Tissue iron accumulation was analyzed using the Iron Stain Kit (Prussian Blue stain, Abcam, ab150674) in accordance with the manufacturer's protocol. Specifically, 5 μm paraffin-embedded liver sections underwent deparaffinization and dehydration. The sections were subsequently incubated in the iron stain solution for 10 min, followed by rinsing with distilled water and counterstaining with hematoxylin. The iron within the tissue sections reacted with acid ferrocyanide to produce a blue coloration. Microscopic images were acquired to document the staining results.

2.7. Histological analyses

Liver tissue samples were subjected to formalin fixation and paraffin embedding. Five-micrometer-thick liver sections were stained with hematoxylin and eosin (H&E). The injured regions were analyzed using a NanoZoomer 2.0-RS whole-slide scanner (Hamamatsu Photonics, Hamamatsu, Japan). For immunohistochemical staining, the antibodies utilized are detailed in Supplemental Table S1. Following heat-induced antigen retrieval and blocking with 5 % normal goat serum, the sections were incubated overnight at 4 °C with primary antibodies. After rewarming to room temperature and washing with PBS, the sections were incubated with biotin-labeled horse anti-mouse/rabbit IgG secondary antibodies for 1 h at room temperature. Finally, the sections were visualized using 3,3′-diaminobenzidine (DAB) and counterstained with hematoxylin.

2.8. Immunofluorescence staining

Liver tissue sections underwent deparaffinization, dehydration, and were treated with heat-induced antigen retrieval. They were then blocked with 5 % normal goat serum. The sections were incubated with primary antibodies overnight at 4 °C, then warmed to room temperature and rinsed with PBS. Subsequently, the sections were incubated with fluorescent-labeled secondary antibodies. Fluorescence microscopy images were acquired using an ECLIPSE Ni-E microscope (Nikon, Japan).

AML12 cells were seeded on coverslips and exposed to RSL3 for 9 h, either as monocultures or cocultures with MSCs, or treated with ML385 or MK-2206. Cells were fixed in 4 % paraformaldehyde for 30 min and permeabilized with 0.3 % Triton X-100 in 3 % BSA for 20 min at room temperature. Following this, cells were blocked with 3 % BSA for 1 h. Next, they were incubated with a primary antibody against *p*-Nrf2 overnight at 4 °C. Cells were then incubated with the appropriate secondary antibody and counterstained with DAPI for 1 h at room temperature, with thorough washing between each step. Confocal laser-scanning microscopy images were captured using an LSM980 microscope (Carl Zeiss, Germany).

2.9. Transmission electron microscopy

Liver tissues were fixed in a solution containing 2.5 % paraformaldehyde and 2.5 % glutaraldehyde in Sorenson's phosphate buffer (pH 7.4). Subsequently, ultrathin sections (50–60 nm) were prepared and mounted on copper grids. The sections were subsequently stained with uranyl acetate and lead citrate to improve contrast, followed by examination using transmission electron microscopy (Hitachi H-7500).

2.10. RNA isolation and quantitative real time PCR

Total RNA was extracted using TRIzol® Reagent (Vazyme) and subsequently reverse-transcribed into cDNA using HiScript II Q RT SuperMix for qPCR (+gDNA wiper) (Vazyme, Catalog No. R223-01). Quantitative real-time PCR (qRT-PCR) assays were conducted to evaluate the relative mRNA expression levels using AceQ® qPCR SYBR Green Master Mix (Vazyme). The mRNA levels of each gene were normalized to the internal control 18S rRNA. Primer sequences utilized in this study are detailed in Supplemental Table S2.

2.11. Bulk RNA-seq analysis of liver tissues from ALF mouse models

Total RNA was extracted from the liver tissues of ALF mouse models using TRIzol® Reagent (Vazyme), and the quality of the RNA was assessed by agarose gel electrophoresis. For RNA-seq, cDNA libraries were generated following the manufacturer's protocol with the MGIEasy RNA Library Prep Kit (catalog number 1000006384, MGI). Subsequently, gene expression profiling was performed on an Illumina HiSeq 2500 instrument. The reads were mapped to the Ensembl Mus musculus (GRCm38. p4) reference genome using HISAT2 software. Differential gene expression (DEG) analysis was performed using DESeq2 to detect genes that were differentially expressed. Upregulated DEGs were used as input for Kyoto Encyclopedia of Genes and Genomes (KEGG) pathway enrichment analysis and Gene Ontology (GO) analysis.

2.12. Immunoprecipitation and immunoblot analysis

For the immunoprecipitation procedure, whole-cell lysates ($n = 3$) were prepared and incubated with the respective antibodies and Protein A/G beads (Pierce) overnight. The beads underwent six washes using a low-salt lysis buffer. Subsequently, the isolated protein was eluted with 1 × SDS loading buffer, fractionated by SDS-PAGE (12.5 %), and then blotted onto PVDF membranes. The membranes were then incubated with the appropriate antibodies (*p*-Nrf2, Akt, ferroportin, and Ub) and detected using an enhanced chemiluminescence (ECL) detection system. The antibodies used in this study are listed in Supplemental Table S1. Protein expression levels were analyzed and quantified using ImageJ software.

2.13. Coculture assays

After obtaining informed consent from the participants, the collection of human umbilical cords was performed. The hUC-MSCs were isolated and cultured as previously described [40]. For coculture assays, 3×10^5 AML12 cells were cocultured with MSCs using a Transwell culture system (0.4 μm pore size, Corning). 1×10^6 MSCs were seeded in the upper chamber. After treatment with RSL3 for 9 h, AML12 cells were cocultured with MSCs for 24 h.

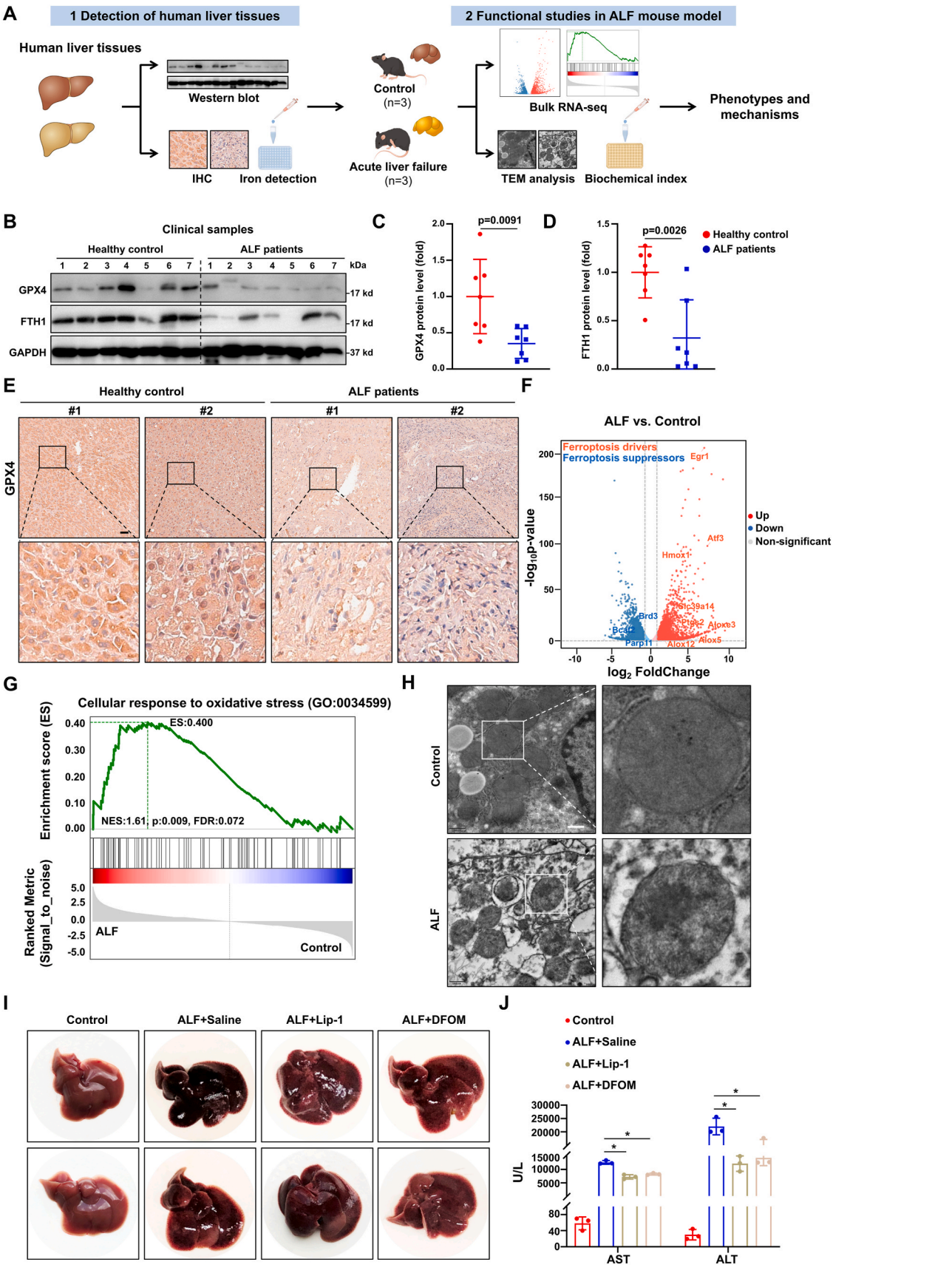

(caption on next page)

Fig. 1. Ferroptosis is implicated in both patients and mouse models of ALF. (A) Workflow illustrating the procedural steps for phenotypic analysis in clinical samples, RNA-seq analysis of liver tissues from healthy controls (n = 3) and ALF mice (n = 3), and mechanistic investigations of potential hepatoprotective strategies. **(B)** Western blotting of GPX4 and FTH1 protein expression in liver tissues from healthy controls (n = 7) and patients with acute liver failure (n = 7). Grayscale scan of GPX4 **(C)** and FTH1 **(D)** protein levels as depicted in (B). **(E)** Immunohistochemical analysis of GPX4 expression in liver tissues from healthy controls and patients with ALF. Scale bar: 50 μm. **(F)** Volcano plot showing the distribution of differentially expressed genes (DEGs) in liver samples from control mice versus those with acute liver failure. **(G)** GSEA demonstrating that the transcriptome of ALF is enriched in genes associated with cellular responses to oxidative stress. **(H)** Representative TEM images of the morphological characteristics of mitochondria in control and ALF liver tissues. Scale bar: 0.5 μm. **(I)** Representative pictures of livers from control and ALF mice treated with vehicle or ferroptosis inhibitors for 12 h. **(J)** Serum levels of AST and ALT in the control group, ALF + Saline group, ALF + Lip-1 group, and ALF + DFOM group (n = 3). All data are presented as means ± SD. $^{*}P < 0.05$, $^{**}P < 0.01$.

2.14. Lipid peroxidation assay

3×10^5 AML12 cells were seeded in 6-well plates and subsequently exposed to RSL3 for 9 h. Following this treatment, the cells were either maintained as monocultures, cocultured with MSCs, or treated with Liproxstatin-1 for 24 h. After this period, cells were washed with PBS and stained with C11-BODIPY (Thermo Fisher Scientific, D3861) at 37 °C for 1 h. Cells were collected and subjected to centrifugation, followed by gentle resuspension in PBS. The fluorescence intensity of the cells was measured using a flow cytometer (BD Biosciences) and a fluorescence microscope (ECLIPSE Ni-E, Nikon, Japan). The data were analyzed using FlowJo software.

Liver sections were incubated with C11-BODIPY, Dihydroethidium (DHE; Abcam, ab236206), or a combination of C11-BODIPY and PK Mito Deep Red (GENVIVO, PKMDR-1) at 37 °C in the dark for 1 h. Subsequently, the samples were washed three times with PBS and counterstained with DAPI (Beyotime, P0131) for nuclear visualization. Fluorescence intensity was quantified using a fluorescence microscope.

2.15. Statistical analysis

Group differences were assessed using unpaired Student t-tests or one-way ANOVA followed by Bonferroni post hoc analyses (performed with GraphPad Prism 9.0, USA). For survival analysis, the Log-rank test was applied. Data are reported as means ± SD. Statistical significance was set at P-values <0.05, unless otherwise stated.

3. Results

3.1. Ferroptosis plays a pivotal role in driving the progression of acute liver failure

To elucidate the role of ferroptosis in the pathogenesis of acute liver failure (ALF), we employed multiple methods to assess the characteristic phenotypes in liver tissues from ALF patients, healthy controls (HCs), and an experimental ALF mouse model (Fig. 1A). Analysis of ferroptosis markers demonstrated that GPX4 and FTH1 in liver tissues from ALF patients (n = 7) were significantly reduced compared to those from healthy controls (n = 7) (Fig. 1B–E). Conversely, PTGS2 mRNA expression was markedly elevated in liver tissues from ALF patients (Supplementary Fig. S1A). These findings indicate that ferroptosis might be a key factor in the development of ALF.

To investigate how ferroptosis contributes to ALF, we established a TAA-induced mouse model and used RNA-seq to analyze liver tissue transcriptomes. A clear separation was observed between the ALF group and the control group in the PCA score plot (Supplementary Fig. S1B). Gene expression analysis revealed high levels of ferroptotic drivers and markers in the ALF group, while ferroptotic suppressors were more prevalent in the control group (Fig. 1F and Supplementary Fig. S1C). Notably, the "cellular response to oxidative stress" category had the most upregulated genes in ALF liver tissues (Fig. 1G). For the validation of ferroptosis phenotypes, in addition to the aforementioned alterations in the expression of specific genes, a critical aspect involves the characteristic morphological changes. Compared to the control group, transmission electron microscopy (TEM) revealed that the mitochondria in the liver tissue of the ALF group exhibited decreased size, higher membrane density, and a reduction or loss of cristae (Fig. 1H). These characteristic alterations provide critical evidence for the occurrence of ferroptosis. In addition, to elucidate the distinct importance of ferroptosis in ALF liver tissue relative to other forms of regulated cell death, we examined the expression levels of genes associated with apoptosis and pyroptosis. Our results indicated that the expression levels of genes related to apoptosis and pyroptosis did not show significant changes in the ALF group (Supplementary Fig. S1D).

Furthermore, to elucidate the pivotal role of ferroptosis in the progression of ALF, we administered ferroptosis-specific inhibitors in mouse model to assess their effects. The results demonstrated that both Lip-1 and DFOM alleviated liver damage, as evidenced by substantial reductions in serum levels of aspartate aminotransferase (AST) and alanine aminotransferase (ALT) (Fig. 1I, J). Notably, based on the results of HE staining of liver tissue (Supplementary Fig. S1E), DFOM, which chelates iron, demonstrates a more pronounced effect in mitigating liver injury compared to Liprostatin-1, which reduces lipid peroxidation. This indicates that modulating iron metabolism and preventing iron overload may be a crucial therapeutic target for treating ALF. Collectively, these results have substantiated the critical significance of ferroptosis in the pathogenesis of ALF and illustrated that inhibiting ferroptosis could be a promising therapeutic strategy.

3.2. Iron overload, caused by a disorder of the hepcidin-ferroportin axis, contributes to ferroptosis in ALF

Ferroptosis is a kind of iron-dependent regulated cell death that is strongly associated with the disruption of iron metabolic homeostasis [12–15,18]. Based on RNA-seq sequencing data from liver tissues of ALF model mice, gene set enrichment analysis (GSEA) indicated a markedly alteration in the expression of genes related to intracellular iron homeostasis in the ALF group. Conversely, the control group exhibited a significant enrichment of genes involved in iron-sulfur cluster binding (Fig. 2A and B), and these genes are of great significance in the regulation of iron metabolism. Furthermore, Perls's Blue Staining and tissue iron detection confirmed elevated iron levels in clinical ALF liver tissues (Fig. 2C and Supplementary Fig. S1F). Consistent findings were observed in the ALF mouse model, with increased liver iron levels, serum NTBI, and hepatic NTBI (Fig. 2D–F). NTBI enters cells, leading to iron overload and subsequently inducing ferroptosis. These data indicate that an imbalance in iron metabolism in the liver leads to iron overload, which subsequently triggers ferroptosis in ALF.

Iron is a critical component that maintains a dynamic homeostasis through continuous uptake, transport, utilization, storage, and circulation within the body. This homeostasis is sustained by a complex and finely orchestrated process [19,20] (Supplementary Fig. S1G). The core of the iron homeostasis regulatory mechanism is centered around the hepcidin-ferroportin (FPN) signaling axis, primarily relying on hepcidin secreted by hepatocytes [19,20]. Interestingly, prior research has documented that ALF patients display distinct alterations in iron parameters, such as hepcidin levels, which not only could serve as an independent predictor of disease outcome but also potentially play a causal role in the development of ALF [21]. FPN, another crucial component in this signaling pathway, is the sole transporter known to facilitate iron export from cells. It is extensively expressed in macrophages and various other cell types. The interaction between ferroportin

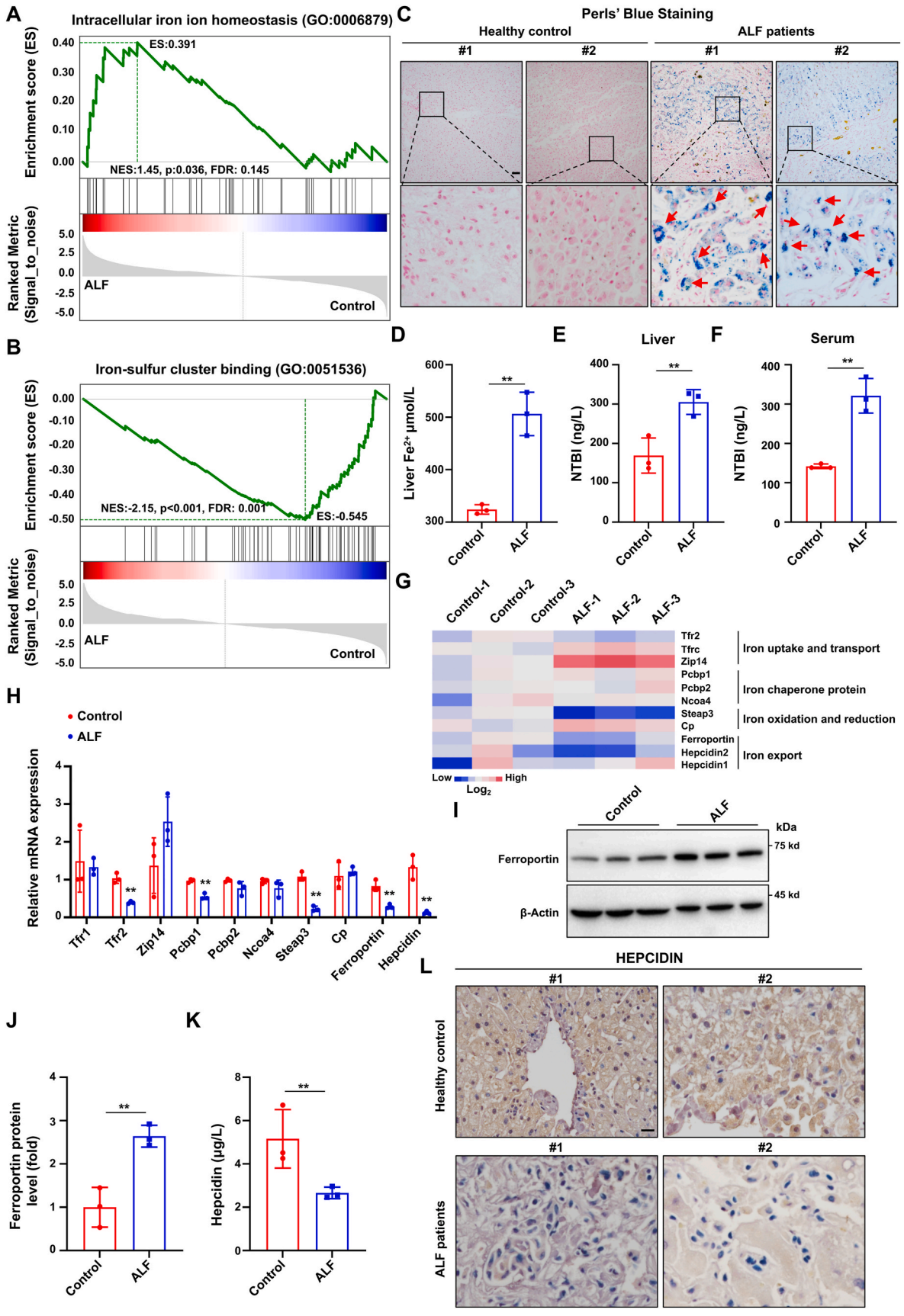

(caption on next page)

Fig. 2. Disruption of iron metabolism triggers ferroptosis in mice with ALF. (A) GSEA plot showing DEGs associated with intracellular iron homeostasis in comparison between the control and ALF groups. **(B)** GSEA plot showing DEGs associated with iron-sulfur cluster binding in comparison between control and ALF groups. **(C)** Perl's Prussian blue staining was performed on 5 μm paraffin-embedded liver sections obtained from healthy controls and patients with ALF. Scale bar: 50 μm. **(D)** Ferrous iron (Fe^{2+}) concentrations were measured in liver tissues from both the control and ALF groups (n = 3 for each group). **(E)** Liver tissue NTBI was quantified in both the control group and the ALF group, with three samples in each group. **(F)** Serum NTBI levels were quantified in control and ALF groups (n = 3). **(G)** Heatmaps illustrating the expression profiles of genes associated with iron metabolism. **(H)** Relative mRNA expression levels of Tfr1, Tfr2, Zip14, Pcbp1, Pcbp2, Ncoa4, Steap3, Cp, Ferroportin and Hepcidin in liver tissues from control and ALF groups (n = 3). **(I)** Immunoblot analysis of Ferroportin expression in liver tissues obtained from control and ALF groups (n = 3). **(J)** Quantification of Ferroportin protein expression in I. **(K)** Hepcidin levels in liver tissue were quantified in the control and ALF group (n = 3). **(L)** Immunohistochemical staining of HEPCIDIN in liver tissues from healthy controls and patients with ALF. Scale bar: 50 μm. All data are presented as means ± SD. $*P < 0.05$, $**P < 0.01$.

and hepcidin triggers the endocytosis and degradation of ferroportin, thus inhibiting iron efflux from cells [25,26,41,42]. In our study, RNA-seq data and qRT-PCR analysis revealed a significant upregulation of Slc39a14 (also known as Zip14), which is crucial for non-transferrin-bound iron (NTBI) uptake into cells, leading to iron overload (Fig. 2G and H). Importantly, we observed a significant downregulation of hepcidin and FPN mRNA levels in the ALF group (Fig. 2G and H). Protein level detection revealed a marked reduction in hepcidin expression and upregulation in ferroportin expression in ALF liver tissue (Fig. 2I–K). Moreover, our subsequent research further demonstrated that in the liver tissues of ALF, ferroportin was predominantly overexpressed in macrophages rather than hepatocytes. In addition, immunostaining analyses further confirmed that hepcidin expression was significantly downregulated in liver tissues from ALF patients relative to healthy controls (Fig. 2L). These findings suggest that the dysfunction of the hepcidin-ferroportin signaling axis may be a critical factor contributing to iron overload in ALF.

3.3. Auranofin activates hepcidin-ferroportin axis to ameliorate ALF

To clarify the role of the hepcidin-ferroportin regulatory axis in iron metabolism disorders and ferroptosis, we hypothesized that activating this axis might inhibit ferroptosis by regulating iron metabolism. Previous research by Professor Fudi Wang's group showed that Auranofin (AUR), an FDA-approved drug for rheumatoid arthritis, effectively promotes hepcidin mRNA expression [43]. However, this study did not assess hepcidin protein levels in the liver tissues of AUR-treated mice. Therefore, we aimed to determine whether AUR could promote hepcidin protein expression and inhibit ferroptosis in ALF with fatal liver dysfunction. ALF mice that received 5 mg/kg body weight of AUR via intraperitoneal injection (Fig. 3A) exhibited alleviation of liver injury, as evidenced by histological examination through HE staining and decreased serum AST and ALT levels (Fig. 3B–E). Additionally, AUR improved the short term survival rate of ALF mice (Supplementary Fig. S2A). Further analysis revealed a substantial downregulation of hepcidin expression in the ALF group, whereas AUR treatment led to a significant upregulation of hepcidin expression at both the mRNA and protein levels (Fig. 3F and G). Consistent results were observed in the ELISA assay (Fig. 3H).

It has been reported that ferroportin is primarily regulated at the post-translational level by hepcidin. Specifically, hepcidin binds to ferroportin, triggering its internalization and then degradation, thereby restricting the amount of iron released from cells [25,26]. Therefore, we further investigated the protein expression and polyubiquitination of ferroportin (FPN) in liver tissues. Our results demonstrated that the protein level of ferroportin (FPN) was significantly elevated in the ALF group, while treatment with AUR markedly reduced ferroportin protein expression and concurrently enhanced its polyubiquitination (Fig. 3I, J and Supplementary Fig. S2E). It is widely recognized that macrophages play a crucial role in restoring and sequestering iron by engulfing damaged red blood cells (RBCs). When needed, they release iron via the iron export protein ferroportin, thus maintaining iron balance. This process is meticulously controlled by the hepcidin-ferroportin axis. In our investigation, we noted a rapid increase in IBA-positive macrophages (MoMFs) surrounding dead hepatocytes following ALF, consistent with the observations made by Professor Gao's group [44]. Importantly, we discovered that ferroportin expression was predominantly localized to these macrophages rather than hepatocytes, and AUR treatment markedly decreased ferroportin levels in macrophages (Fig. 3K and Supplementary Fig. S2D). These findings indicate that modulating the hepcidin-ferroportin regulatory axis could represent a potential therapeutic approach for the management of ALF. So, is Auranofin the optimal choice for treating ALF?

Previous studies have shown that short-term administration of AUR not only increases the expression of hepcidin mRNA in the liver but also that of interleukin-6 (IL-6) [43]. Consequently, we analyzed the expression levels of inflammatory cytokines and chemokines. The findings revealed that, compared with untreated ALF mice, the mRNA levels of Il6 and Cxcl1 were significantly elevated in the AUR-treated group, whereas the expression of Ccl2 was reduced, and there was no notable impact on Cxcl10 expression (Supplementary Fig. S2B). Furthermore, ELISA confirmed a substantial increase in the serum IL-6 protein level in ALF mice following AUR treatment (Supplementary Fig. S2C). However, during the progression of ALF, disorder of the immune system is particularly pronounced, and the inflammatory response plays a critical role in disease progression [2]. A significant amount of inflammatory factors, such as IL-6, released after hepatocyte death can trigger excessive immune activation, leading to systemic inflammatory response syndrome (SIRS) [45]. These inflammatory responses are not confined to the liver but also affect other organ systems, contributing to multiple organ dysfunction, which is a major factor in the high mortality rate associated with ALF [2,46]. Given these findings, the elevated IL-6 expression induced by AUR may not be beneficial for improving overall prognosis and liver function in ALF patients, particularly in the long term. Therefore, we pose the question: is there a more suitable treatment option than Auranofin? This question merits further investigation to develop more effective treatment strategies for ALF patients.

3.4. MSCs activates hepcidin-ferroportin axis to maintain iron homeostasis

It is widely acknowledged that iron homeostasis in the body represents a dynamic equilibrium process. Key regulators of iron metabolism, such as hepcidin and ferroportin, must function within an optimal range to maintain iron balance. Both excessively high and low levels of hepcidin can disrupt iron homeostasis, thereby adversely impacting overall health. A clinical study on Rusfertide (a hepcidin mimetic) has shown that hepcidin agonists may be associated with a series of side effects, some of which are potentially life-threatening [47]. Therefore, the cornerstone of treating iron-related diseases lies in restoring and maintaining iron homeostasis rather than merely modulating specific components. A mild yet potent modulator, rather than a simple agonist or analogue of hepcidin, would more effectively restore iron homeostasis in ALF. Mesenchymal stromal cells (MSCs), a type of adult stem cell with multi-target and multi-functional properties, exhibit potent secretory and proliferative capabilities. They protect the liver by mechanisms including the inhibition of inflammatory responses, modulation of immune function, suppression of apoptosis, and promotion of cell proliferation [32–34]. These features position MSCs as a highly promising candidate for achieving this therapeutic objective. Our previous studies

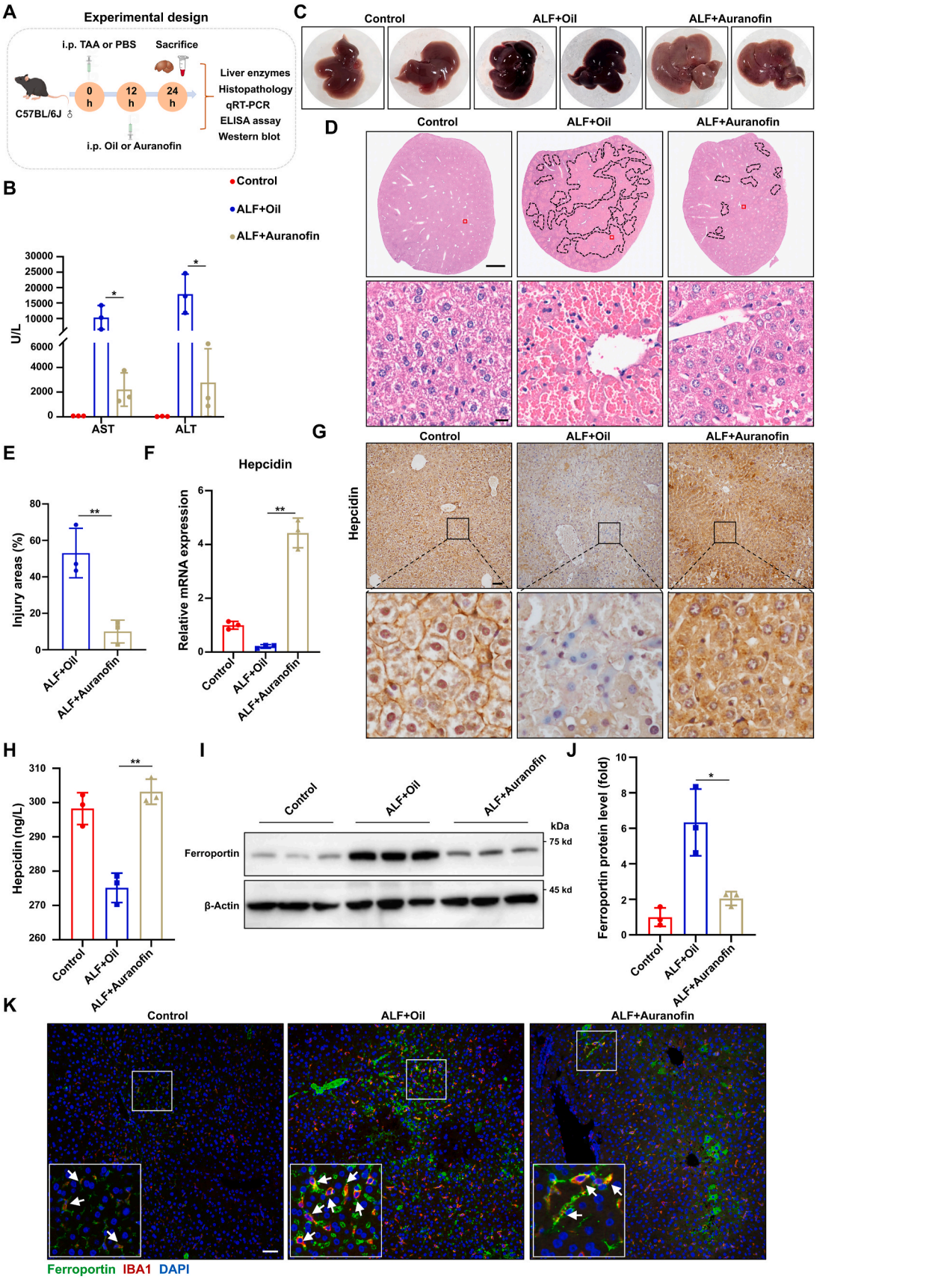

(caption on next page)

Fig. 3. Acute Auranofin administration enhances hepcidin expression and mitigates hepatic injury in mice with ALF. (A) Schematic illustration of the protocol for inducing ALF in mice and subsequent Auranofin administration. **(B)** Serum AST and ALT levels in the control group, ALF + Oil group, and ALF + Auranofin group (n = 3). **(C)** Representative gross specimens of livers from the control, ALF + Oil, and ALF + Auranofin groups. **(D)** Hematoxylin and eosin (H&E)-stained liver sections, visualized at magnifications of × 1.25 and × 20. Scale bar: 500 μm, 50 μm. **(E)** The proportion of injured regions was quantified (n = 3). **(F)** mRNA expression levels of Hepcidin in liver tissues from control, ALF + Oil, and ALF + Auranofin groups (n = 3). **(G)** Immunohistochemical staining of hepcidin was performed on liver tissues obtained from three groups: control, ALF treated with oil, and ALF treated with auranofin. Scale bar: 50 μm. **(H)** Hepcidin levels in liver tissue were quantified in the control group, the ALF + Oil group, and the ALF + Auranofin group (n = 3). **(I)** Immunoblot analysis of Ferroportin expression in liver tissues from control, ALF + Oil, and ALF + Auranofin groups (n = 3). **(J)** Quantification of Ferroportin expression in I. **(K)** Immunofluorescent staining of IBA1 and Ferroportin was performed on liver sections derived from the control, ALF + Oil, and ALF + Auranofin groups. Scale bar: 50 μm. All data are presented as means ± SD. $^{*}P < 0.05$, $^{**}P < 0.01$.

have shown that transplantation of mesenchymal stromal cells (hUC-MSCs) derived from human umbilical cord can effectively alleviate acute liver injury caused by acetaminophen (APAP) [48] or concanavalin A (Con A) [36,49]. Not surprisingly, our results demonstrated that MSCs infusion significantly inhibited the activation of the IL-17 signaling pathway in TAA-induced ALF mice (Supplementary Fig. S3A). Additionally, we measured cytokine expression levels and found that serum levels of IL-6 and MCP-1 were elevated significantly, which could be mitigated by MSCs infusion (Supplementary Fig. S3B and C). These findings indicate that MSCs can compensate the above-mentioned disadvantage of Auranofin, specifically the unexpectedly elevated inflammatory factors. However, the precise mechanism by which MSCs repair liver injury remains not fully elucidated, particularly from the perspective of iron metabolism. Based on the aforementioned experimental results, we hypothesized that MSCs might alleviate ALF by regulating the hepcidin-ferroptotin signaling axis and maintaining iron metabolism homeostasis. Firstly, our findings demonstrated that MSCs treatment significantly increased the mRNA levels of hepcidin and ferroportin relative to those in the ALF group (Fig. 4A). Then we found that MSCs infusion led to a significant rescue in hepcidin expression at protein level (Fig. 4B–D). Conversely, the protein level of ferroportin was significantly elevated in the ALF group, whereas MSCs treatment markedly downregulated ferroportin protein expression (Fig. 4E, F and Supplementary Fig. S3D). Given that ferroportin protein levels are regulated by hepcidin at the post-translational level, we further examined whether the reduction in ferroportin protein in MSCs-treated ALF mice was due to enhanced polyubiquitination. Not coincidentally, our findings indicated that MSCs treatment increased the polyubiquitination of ferroportin (Fig. 4G). These data suggest that MSCs treatment modulates the hepcidin-ferroportin axis. Next, we investigated whether activation of the hepcidin-ferroportin axis by MSCs could maintain iron homeostasis. As anticipated, we observed a remarkable reduction in serum and hepatic non-transferrin-bound iron (NTBI) levels in the group receiving MSCs infusion (Fig. 4H–J). Collectively, our data indicate that MSCs treatment significantly alleviates iron overload in TAA-induced ALF, at least in part, through the hepcidin-ferroportin axis.

3.5. *MSCs regulate hepcidin expression in a PI3K/Akt/Nrf2-dependent manner*

To investigate the molecular mechanisms through which MSCs influence the hepcidin-ferroportin axis, we analyzed the gene expression profile of liver tissue from mice with ALF. A total of 969 upregulated differentially expressed genes (DEGs) were identified in the MSCs treatment group compared to the ALF group. To further assess the potential core transcription factors (TFs) involved in the regulation of the hepcidin-ferroportin axis in the MSCs treatment group, we inputted the 969 upregulated DEGs, along with ferroptosis-related drivers, markers, and suppressors, into the TRRUST database. Overlap analysis revealed that 39 overlapping TFs were obtained, including Nrf2, Tp53, Nfκb, Sp1, Stat3, Ep300, Jun, Egr1, and others (Fig. 5A and Supplemental Table S3 and S4). Consistent with these findings, qRT-PCR analyses showed that MSCs treatment restored the expression of Nrf2, Tp53, Sp1, and Stat3 (Fig. 5B). Of note, Nrf2, a well-known regulator of antioxidant responses and iron metabolism, has been reported to stimulate hepcidin expression upon activation, thereby maintaining iron homeostasis, which may serve as a therapeutic target for iron-related diseases [50–52]. Based on these findings, we hypothesize that there might be a connection between Nrf2 and hepcidin following MSCs treatment. To investigate this, we analyzed the phosphorylation levels of Nrf2 (*p*-Nrf2) in liver tissues from each group and found that MSCs treatment significantly elevated the levels of *p*-Nrf2 compared to those in the ALF group (Fig. 5C and D). Coincidentally, AUR treatment resulted in a significant increase in the levels of *p*-Nrf2 (Supplementary Fig. S2F and G). Additionally, gene expression profiling demonstrated that several Nrf2 downstream genes were upregulated following MSCs treatment (Supplementary Fig. S5A). Next, we aimed to identify the upstream regulators of *p*-Nrf2. KEGG enrichment analysis revealed that the Rap1-PI3K-Akt signaling pathway was markedly enhanced following MSCs treatment (Supplementary Fig. S5B). At the protein level, immunohistochemistry analysis confirmed that MSCs treatment significantly upregulated the expression of phosphorylated Akt (Supplementary Fig. S5C). Furthermore, to investigate the potential regulatory relationship between Nrf2 and Akt, we performed co-IP and immunoblot assays. The results demonstrated that the association between *p*-Nrf2 and Akt was significantly enhanced following MSCs treatment (Fig. 5E).

To further substantiate these findings, we developed an *in vitro* coculture system wherein AML12 cells were exposed to either DMSO or RSL3, followed by monoculture or coculture with MSCs, with parallel groups receiving Liproxstatin-1 (Lip-1) treatment for 24 h (Supplementary Fig. S4A). AML12 cells treated with RSL3, a known ferroptosis inducer, exhibited a notable increase in the characteristic "ballooning" morphology associated with ferroptotic cell death. Both MSCs coculture and Lip-1 treatment significantly mitigated RSL3-induced ferroptosis, as evidenced by a marked reduction in the number of cells undergoing ferroptosis (Supplementary Fig. S4B and C). Furthermore, the expression of Gpx4 protein was found to be elevated in AML12 cells either cocultured with MSCs or treated with Lip-1 (Supplementary Fig. S4D and E). Consistent with these findings, RSL3 administration resulted in a significant increase in lipid-ROS levels, which were comparably attenuated by MSCs coculture or Lip-1 treatment (Supplementary Fig. S4F–H). Collectively, these data indicate that MSCs exert an inhibitory effect on ferroptosis *in vitro*.

Next, in order to investigate whether MSCs inhibit ferroptosis by modulating the PI3K/Akt/Nrf2 signaling pathway, we performed *in vitro* experiments and demonstrated that treatment with the ferroptosis inducer RSL3 led to a significant reduction of *p*-Nrf2 accumulation in the nucleus. However, MSCs not only upregulated the phosphorylation levels of Nrf2 (*p*-Nrf2) and Akt (*p*-Akt) (Fig. 5F and G), but also facilitated the translocation of *p*-Nrf2 into the nucleus (Fig. 5H and I). To further confirm whether there is a direct causal relationship between Nrf2 signaling and hepcidin expression mediated by MSCs, we evaluated the recovery of liver injury and hepcidin expression in ALF mice treated with MSCs with or without the presence of ML385, a well-tolerated Nrf2 inhibitor (Fig. 6A). As expected, treatment with ML385 counteracted the therapeutic effects of MSCs in ALF mice, as evidenced by serum levels of AST, ALT, and HE staining (Fig. 6B–D). Consistently, ML385 treatment downregulated hepcidin expression in ALF mice treated with MSCs (Fig. 6E and F). Additionally, inhibition of Akt and Nrf2 reduced *p*-Nrf2 nuclear accumulation in AML12 cells co-cultured with MSCs

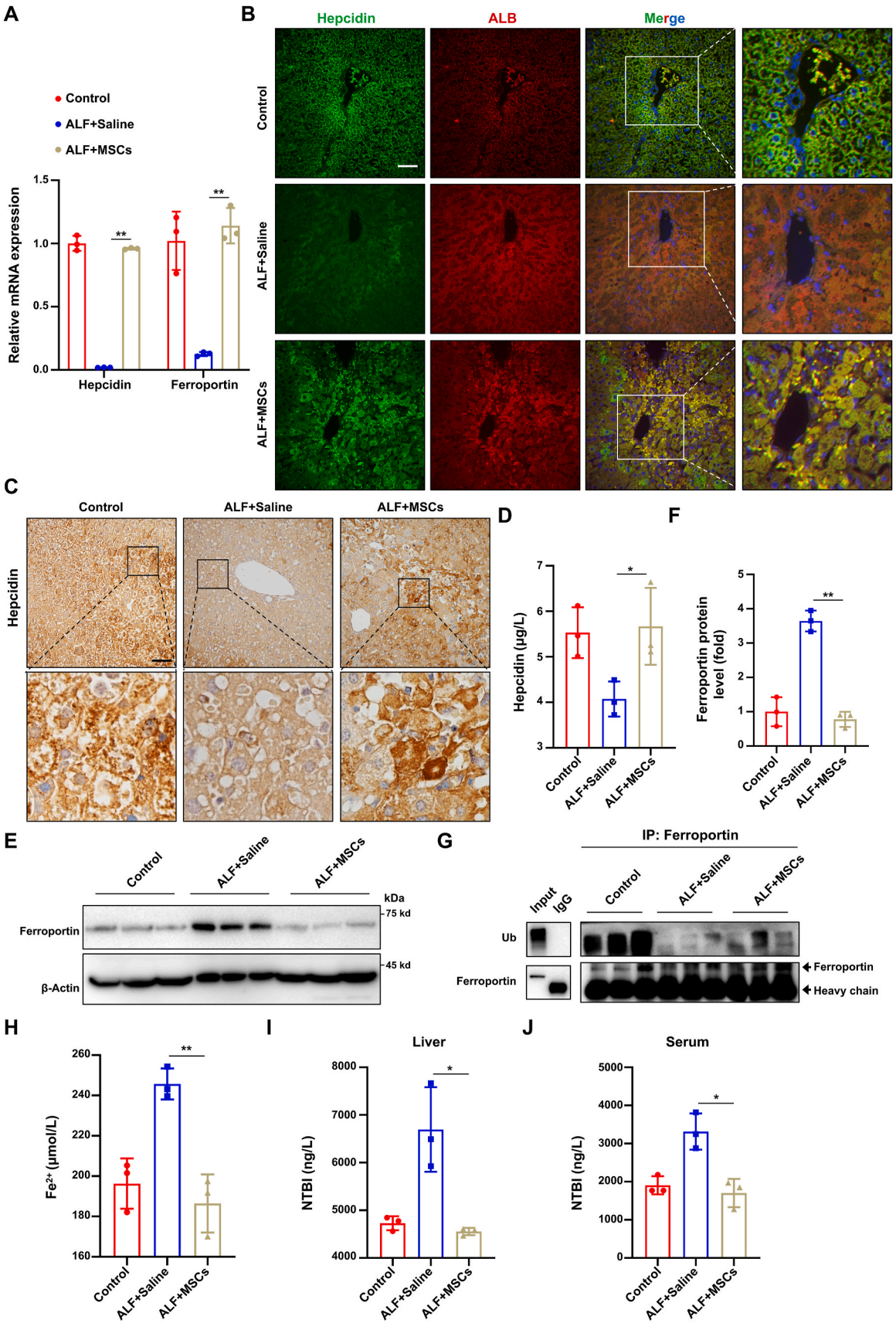

(caption on next page)

Fig. 4. MSCs regulate the hepcidin-ferroportin axis to maintain iron homeostasis. **(A)** mRNA levels of Hepcidin and Ferroportin in liver tissues from control, ALF + Saline and ALF + MSCs groups (n = 3). **(B)** Representative immunofluorescence staining was conducted to assess hepcidin expression in hepatocytes from three groups: control, ALF + Saline, and ALF + MSCs. Scale bar: 20 μm. **(C)** Immunohistochemical staining of hepcidin in liver tissues from three groups: control, ALF treated with saline, and ALF treated with MSCs. Scale bar: 20 μm. **(D)** Hepcidin concentrations in liver tissue were quantified using ELISA in three groups: the control group, the ALF + Saline group, and the ALF + MSCs group (n = 3). **(E)** Immunoblot analysis of Ferroportin expression in liver tissues from control, ALF + Saline, and ALF + MSCs groups (n = 3). **(F)** Quantification of Ferroportin expression via greyscale scanning in (E). **(G)** The liver tissue lysates were subjected to immunoprecipitation (IP) with anti-Ferroportin or IgG as a negative control and immunoblot analysis with anti-ubiquitin (n = 3). **(H)** Ferrous iron (Fe^{2+}) concentrations were detected in liver tissues of the control, ALF + Saline and ALF + MSCs groups (n = 3). **(I)** Liver tissue NTBI was measured in control, ALF + Saline and ALF + MSCs groups (n = 3). **(J)** Serum NTBI was measured in control, ALF + Saline and ALF + MSCs groups (n = 3). All data are presented as means ± SD. $^{*}P < 0.05$, $^{**}P < 0.01$.

(Supplementary Fig. S6A). All together, these findings suggest that MSCs promote hepcidin expression through a PI3K/Akt/Nrf2-dependent mechanism.

3.6. MSCs inhibits ferroptosis to alleviate ALF

Based on the above findings, we have established that the disruption of the hepcidin-ferroportin axis plays a critical role in ferroptosis in ALF mice. Moreover, mesenchymal stromal cells (MSCs) transplantation activates hepcidin, thereby maintaining iron homeostasis through the regulation of the PI3K/Akt/Nrf2 signaling pathway. To further explore whether MSCs treatment can inhibit ferroptosis and alleviate ALF, we conducted additional experiments. As anticipated, mice treated with MSCs exhibited reduced liver injury compared to the control group, as evidenced by lower serum AST and ALT levels (Fig. 7A). Consistent with this, treatment with MSCs markedly enhanced the survival rate of mice with ALF (Fig. 7B). We then assessed the expression of ferroptosis markers in liver tissues from each group. The results demonstrated that the mRNA levels of Gpx4 were significantly downregulated, while those of Hmox1, Ptgs2, and Slc7a11 were upregulated in ALF mice. However, MSCs treatment markedly restored Gpx4 expression and reduced the expression of Hmox1, Ptgs2, and Slc7a11 (Fig. 7C). Similar trends were also observed at the protein level. Following MSCs infusion, the protein levels of Transferrin receptor (Tfrc), Gpx4, and Fth1 were significantly increased compared to those in the ALF group (Fig. 7D and E). Immunostaining further validated these observations (Fig. 7F and Supplementary Fig. S7A). To evaluate oxidative stress in liver tissues, we conducted C11-BODIPY and DHE staining for ROS detection. The results demonstrated that ROS production was significantly higher in the ALF group than in the control group, while MSCs treatment effectively attenuated ROS production (Supplementary Fig. S7B). Moreover, subcellular localization analysis demonstrated that the elevated ROS predominantly accumulated in the mitochondria, and MSCs infusion significantly mitigated mitochondrial lipid peroxidation (Fig. 7G). Additionally, transmission electron microscopy (TEM) revealed that mitochondria in the MSC-treated group showed signs of normalization compared to the ALF group (Fig. 7H). Collectively, these results indicate that MSCs treatment effectively mitigates ALF by inhibiting ferroptosis.

4. Discussion

Acute liver failure is a grave condition characterized by abrupt occurrence, rapid progression, and high fatality rates [1,2,10]. It can lead to various metabolic dysfunctions, such as disruptions in iron metabolism, thereby exacerbating the progression of ALF. In the current study, our findings indicate that ferroptosis is a critical pathophysiological mechanism in the development of ALF. Mechanistically, the dysregulation of hepcidin-ferroportin axis results in iron overload, thus triggering ferroptosis in the liver. Interestingly, we identified a novel therapeutic application of Auranofin, an anti-rheumatic drug, which exerts hepatoprotective effects by upregulating hepcidin. More importantly, our results demonstrated that MSCs rectify iron metabolism disorders and inhibit ferroptosis by activating hepcidin-ferroportin axis, and effectively alleviate ALF.

Previous studies have suggested that apoptosis and pyroptosis are the predominant forms of cell death in ALF [7–9,11]. Even earlier studies support oncotic necrosis as the primary mode of cell death, though some overlap with apoptosis, pyroptosis and ferroptosis signaling events fuels ongoing debates [6]. Although inhibitors targeting these modes of cell death may offer protective effects in experimental models, no specific pharmacological inhibitors have been applied clinically to date. Therefore, further research is essential to elucidate additional and comprehensive mechanisms underlying ALF pathogenesis. Notably, the liver exhibits a high susceptibility to ferroptosis. First, the liver's critical role in iron storage and regulation predisposes it to abnormal iron metabolism and accumulation, creating an environment conducive to ferroptosis [19]. Second, the liver's rich lipid content serves as a substrate for lipid peroxidation and influences the activity of lipid metabolic enzymes involved in ferroptosis. Additionally, the liver's active metabolism and detoxification functions expose it to oxidative stress, which further promotes ferroptosis [15,18]. Consequently, ferroptosis is closely linked to the pathogenesis and progression of various liver diseases. Our studies, along with those of other research groups, have demonstrated the potential of ferroptosis inhibitors in mitigating liver injury. Targeted modulation of ferroptosis is anticipated to emerge as a novel therapeutic strategy for liver diseases.

Some studies have shown that disorders of iron metabolism play an important role in the pathogenesis and progression of certain liver diseases, such as hereditary hemochromatosis (HH) and non-alcoholic fatty liver disease [14,15,18]. In the context of acute chemical or drug-induced liver injury/liver failure, existing literature mainly investigates the process of ferroptosis from the perspective of oxidative damage and impairment to antioxidant systems. For example, in carbon tetrachloride (CCl4)-induced acute liver injury, GPX4 and SLC7A11 are inhibited, impairing the liver's ability to scavenge reactive oxygen species (ROS), resulting in lipid peroxidation and a large number of liver cells undergoing ferroptosis [53]. Additionally, acetaminophen (APAP) overdose, representing as the most common cause of ALF in many countries, leads to decreased levels of glutathione (GSH) within hepatocytes, accompanied by increased lipid peroxidation [6]. Similar phenomena have also been observed in mouse models of ALF induced by lipopolysaccharide (LPS) and D-galactosamine (GalN) [8]. Based on these findings, some scholars have proposed the development of antioxidant therapies as a promising treatment strategy for ALF. However, others have challenged this notion, arguing that antioxidants alone are insufficient to effectively mitigate the systemic inflammatory response syndrome (SIRS) associated with ALF [45,46]. Nonetheless, disorders of iron metabolism, a critical biochemical process driving ferroptosis in ALF, have not received comparable attention. A clinical study revealed significant alterations in iron metabolism parameters among patients with ALF, primarily characterized by reduced serum hepcidin levels, an independent predictor of ALF outcomes [21]. Consistent with these findings, our study also identified decreased hepcidin levels in ALF liver tissue. Furthermore, we demonstrated that upregulating hepcidin expression via Auranofin administration or MSCs transfusion exerts beneficial effects on alleviating ALF. However, an unexpected increase in inflammatory factors, such as IL-6, was observed following Auranofin treatment. While IL-6 is known to initiate hepatocyte proliferation through JAK-STAT3, PI3K/Akt, and YAP/Notch pathways to promote cell cycle entry and DNA synthesis, thereby playing a potential role in liver regeneration, it cannot be overlooked that during acute liver injury, elevated IL-6 levels mediate inflammation by activating

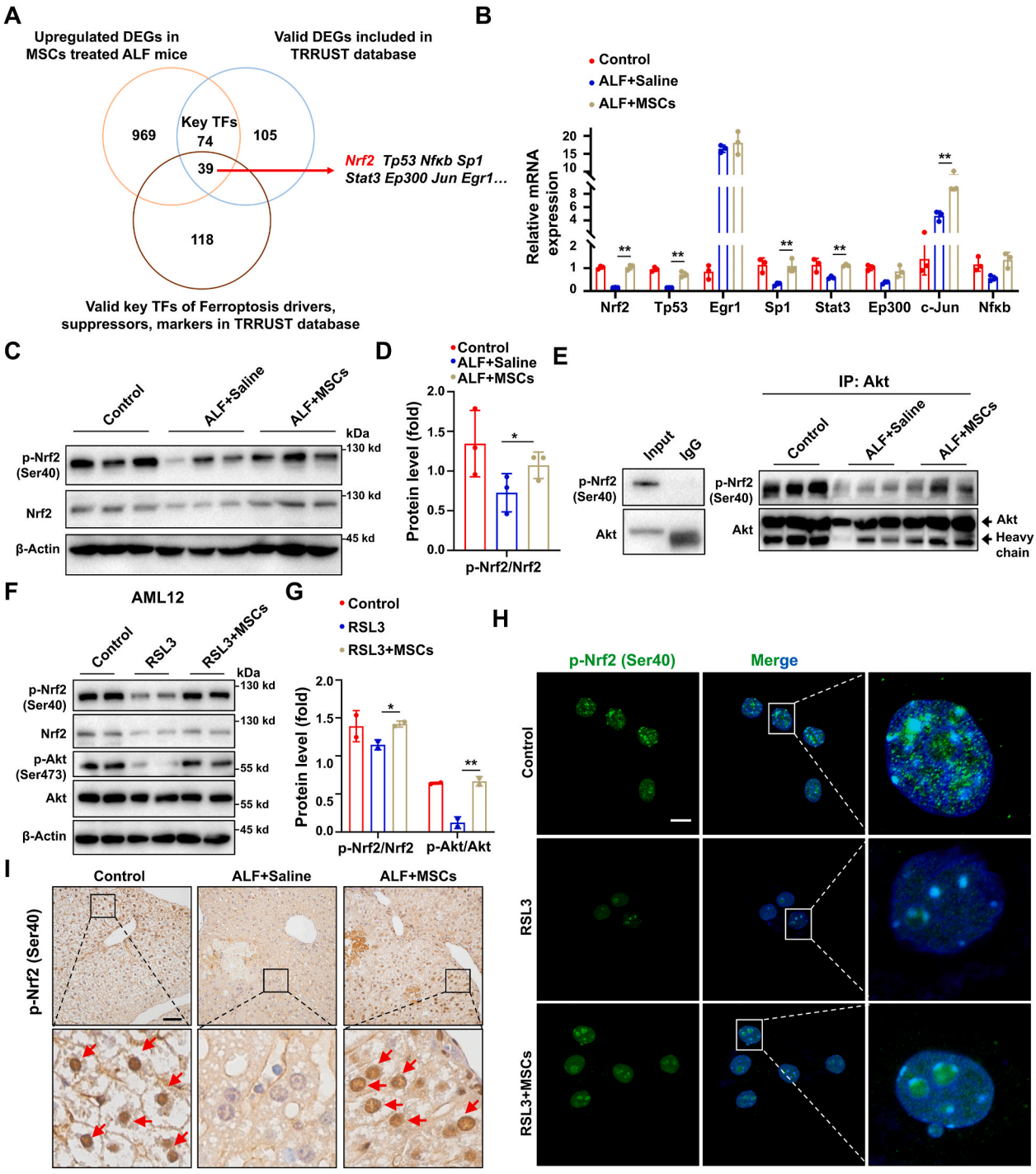

Fig. 5. PI3K/Akt/Nrf2 signaling pathway mediates hepcidin expression induced by MSCs treatment. (A) Venn diagram illustrating the intersection of transcription factors (TFs) in upregulated DEGs from MSCs-treated ALF mice and genes associated with ferroptosis. **(B)** qRT-PCR was employed to validate the expression levels of several candidate transcription factors (TFs) in liver tissues obtained from the control, ALF + Saline and ALF + MSCs groups (n = 3). **(C)** Immunoblot analysis of phosphorylated Nrf2 (*p*-Nrf2) and total Nrf2 in liver tissues obtained from control, ALF + Saline, and ALF + MSCs groups (n = 3). **(D)** Quantification of *p*-Nrf2 expression via greyscale scanning in (C). **(E)** Liver tissue lysates were subjected to immunoprecipitation (IP) using anti-Akt antibodies, with IgG serving as a negative control, followed by immunoblot analysis with anti-*p*-Nrf2 antibodies. **(F)** AML12 cells were treated with RSL3 for 9 h, followed by monoculturing or co-culturing with MSCs for an additional 24 h. Subsequently, immunoblot analysis was conducted to examine the levels of *p*-Nrf2, Nrf2, *p*-Akt, and Akt. **(G)** Quantification of *p*-Nrf2 and *p*-Akt expression via greyscale scanning is presented in (F). **(H)** Microscopy was performed on AML12 cells that were treated with RSL3 and either monocultured or cocultured with MSCs for 24 h, followed by immunostaining of phosphorylated Nrf2 (*p*-Nrf2) using a specific primary antibody (stained green). Nuclei were counterstained with DAPI (blue). Scale bar: 20 μm. **(I)** Immunohistochemical analysis of *p*-Nrf2 expression in liver tissues from control, ALF + Saline, and ALF + MSCs groups. Scale bar: 20 μm. All data are presented as means ± SD. $^{*}P < 0.05$, $^{**}P < 0.01$.

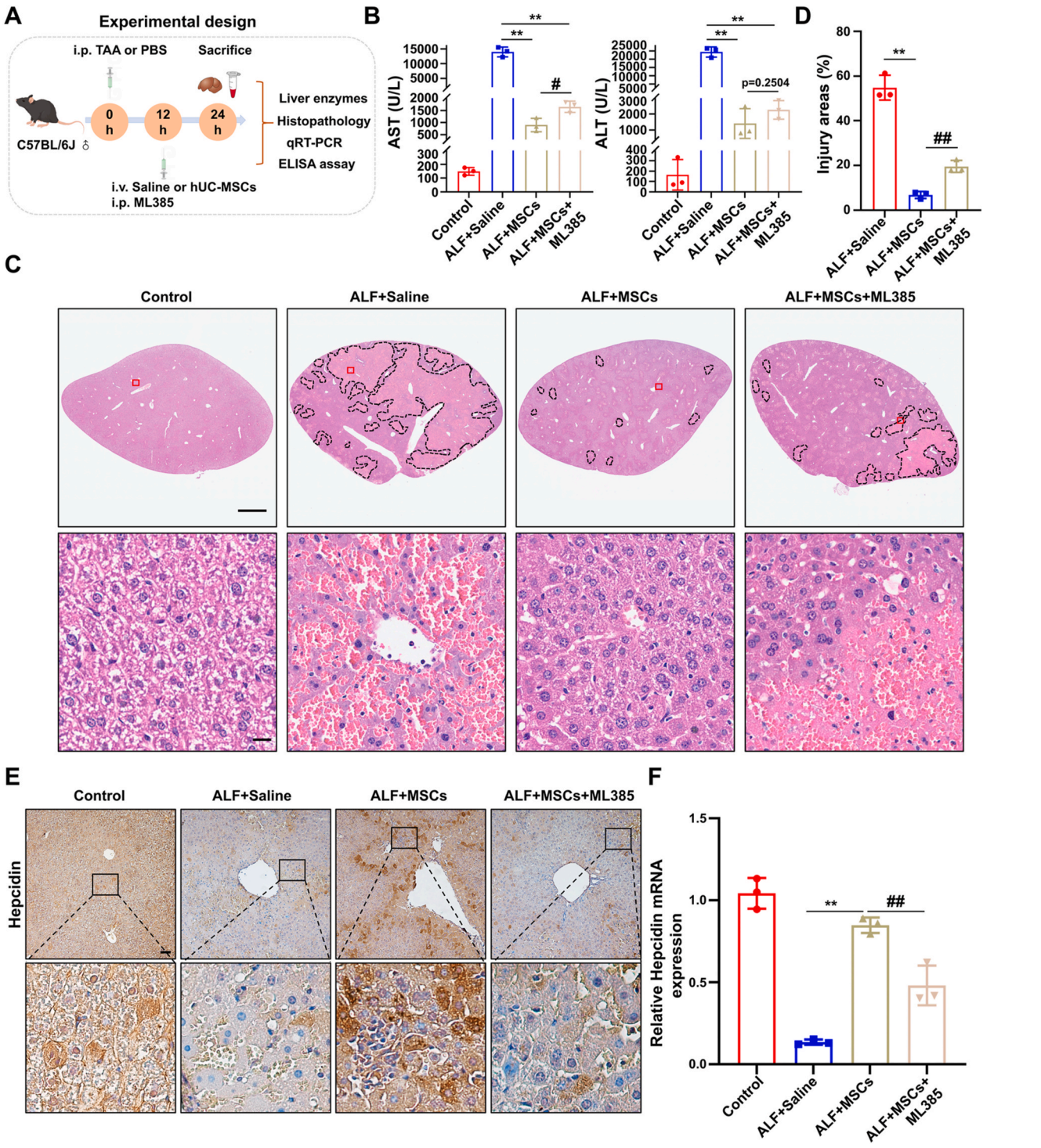

Fig. 6. Inhibition of Nrf2 impairs the recovery from liver injury and hampers hepcidin expression mediated by MSCs. (A) Schematic diagram of ALF mice treated with vehicle, MSCs or Nrf2 inhibitors (ML385). **(B)** Serum AST and ALT levels were measured in the control group, ALF + Saline group, ALF + MSCs group, and ALF + MSCs + ML385 group (n = 3). **(C)** Hematoxylin and eosin (H&E)-stained liver sections examined at × 1.25 and × 20 magnification. Scale bar: 500 μm, 50 μm. **(D)** The percentage of injured areas was quantified in three independent samples (n = 3). **(E)** Immunohistochemical staining of hepcidin in liver tissues obtained from control, ALF + Saline, ALF + MSCs, and ALF + MSCs + ML385 groups. Scale bar: 50 μm. **(F)** mRNA levels of hepcidin in liver tissues from control, ALF + Saline, ALF + MSCs, and ALF + MSCs + ML385 groups (n = 3). All data are presented as means ± SD. $^{*}P < 0.05$, $^{**}P < 0.01$. $\#P < 0.05$, $\#\#P < 0.01$.

non-parenchymal cells such as macrophages, T cells, and hepatic stellate cells via NF-κB and STAT3 pathways, potentially exacerbating hepatic damage at high concentrations or with persistent elevation [54]. Given that Auranofin exhibits the adverse effect of upregulating the expression of inflammatory factors, it is imperative to reassess its clinical application and develop optimal alternatives for the treatment of ALF. It is noteworthy that despite the observation of excess iron accumulation in patients with acute liver failure, this does not necessarily indicate that reducing iron levels would be beneficial. Considering iron's essential role in human health, therapeutic strategies for acute liver failure should focus on restoring or maintaining iron homeostasis. Given that iron homeostasis is regulated by the coordinated action of multiple key

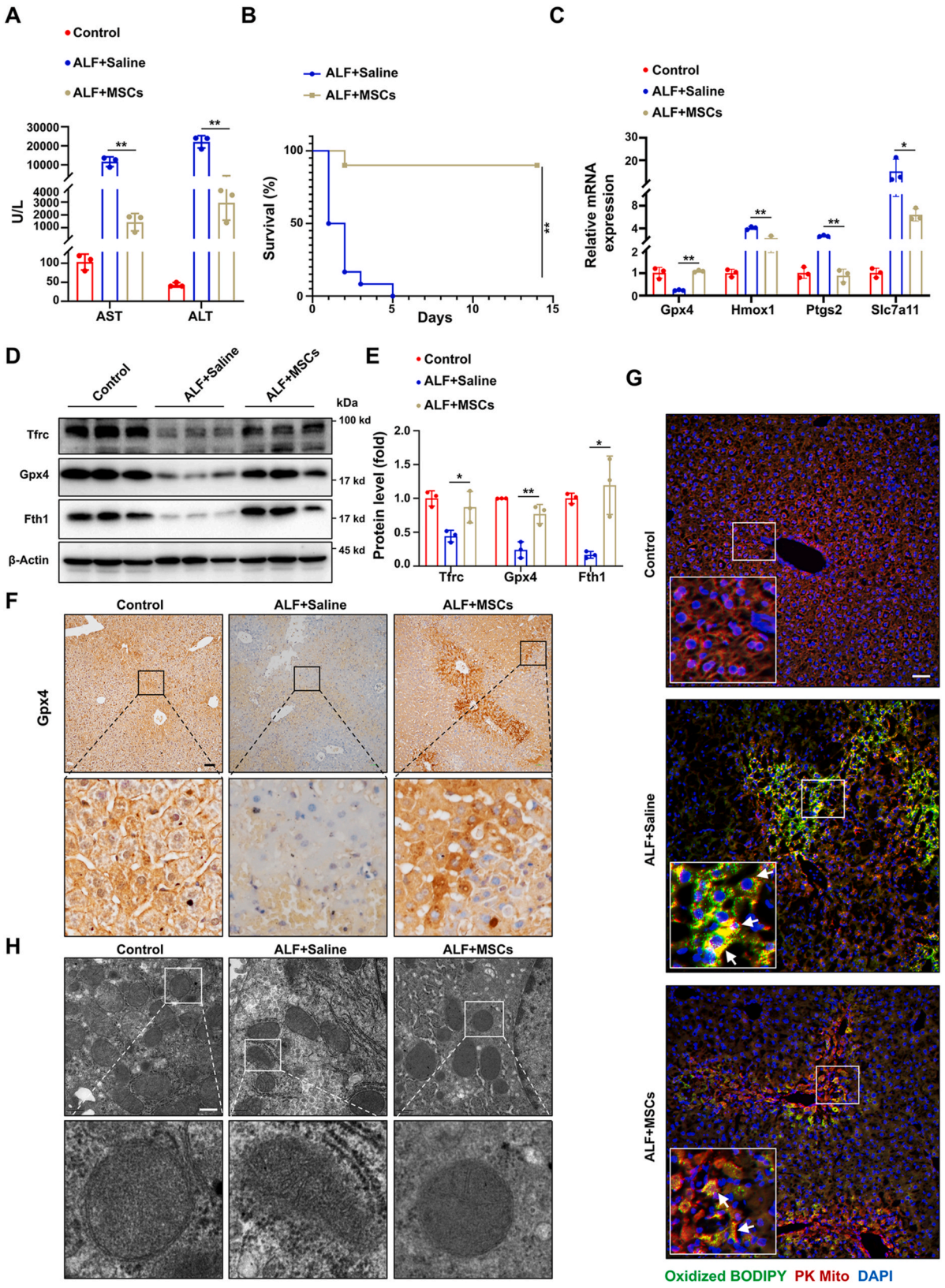

Fig. 7. Treatment with MSCs inhibits ferroptosis, thereby alleviating ALF. (A) Serum AST and ALT levels in the control group, the ALF + Saline group, and the ALF + MSCs group (n = 3). **(B)** Survival curves of mice in the ALF + Saline and ALF + MSCs groups. **(C)** mRNA levels of Gpx4, Hmox1, Ptgs2 and Slc7a11 in liver tissues from control, ALF + Saline and ALF + MSCs groups (n = 3). **(D)** Immunoblot analysis of Tfrc, Gpx4 and Fth1 protein expression in liver tissues from control, ALF + Saline, and ALF + MSCs groups (n = 3). **(E)** Quantification of Tfrc, Gpx4 and Fth1 expression levels was performed through greyscale scanning as shown in (D). **(F)** Immunochemical analysis of Gpx4 expression in liver tissues from control, ALF + Saline, and ALF + MSCs groups. Scale bar: 50 μm. **(G)** Liver tissues were probed with C11-BODIPY and PK-mito. Scale bar: 50 μm. **(H)** Representative TEM images illustrating the mitochondrial morphology in the control, ALF + Saline, and ALF + MSCs groups. Scale bar: 0.5 μm. All data are presented as means ± SD. $^{*}P < 0.05$, $^{**}P < 0.01$.

molecules and signaling pathways, achieving this goal may prove challenging with compounds or drugs targeting only a single or fixed target. Compared to traditional single-target or fixed-target small molecule compounds, multi-target therapeutic strategies such as MSCs therapy may provide unparalleled advantages in the treatment of complex clinical syndromes like ALF.

MSCs, referred to as mesenchymal stromal cells or medicinal signaling cells, exhibit significant potential in regenerative medicine [55]. This potential is attributed to their unique characteristics, such as diverse origins, minimal ethical concerns, low immunogenicity, and robust secretory functions that surpass their self-renewal and differentiation capabilities. Importantly, MSCs possess chemotactic migration properties, the ability to mitigate oxidative damage, suppress inflammation, promote cell proliferation, and exert immunomodulatory effects, positioning them as a promising therapeutic option for liver diseases [29,31–34]. Based on the antioxidant properties of MSCs, Feiyan Lin et al. demonstrated that these cells maintain SLC7A11 stability, thereby activating system XC^- and ultimately inhibiting ferroptosis [53]. However, the role of MSCs in modulating iron metabolism for the treatment of ALF has been underexplored in previous studies. Notably, our findings indicate that MSCs regulate iron metabolism via the hepcidin-ferroportin axis to inhibit ferroptosis, offering a novel perspective distinct from prior research. Nonetheless, further investigation is required to fully elucidate the effector molecules involved in MSC-mediated regulation of iron metabolism-related signaling pathways.

The findings from our research group [35,36,48,49] and other investigators [31,37,53] have provided substantial evidence supporting the remarkable hepatoprotective role of MSCs. Their safety and efficacy have been validated through extensive clinical trials [35,37–39]. Consequently, MSCs have demonstrated considerable therapeutic potential and broad application prospects in the treatment of ALF (29, 31–33). Notably, on December 18, 2024, the FDA granted approval for an MSC-based therapy to treat steroid-resistant acute graft-versus-host disease (SR-aGVHD), marking the world's first allogeneic "off--the-shelf" cell therapy approved by the FDA. This represents a significant milestone in the clinical application of MSCs therapy. Beyond the FDA-approved indications for GVHD, further in-depth fundamental research is essential to fully explore the potential of MSCs therapy in treating ALF. Precise indication selection and the design of appropriate intervention strategies are critical for the success of MSCs clinical research. Specifically, several key factors must be considered: the source of MSCs, the optimal therapeutic time window for MSCs administration, the dosage per transfusion, the frequency and intervals between transfusions, and whether MSCs should undergo pretreatment or genetic modification to enhance efficacy. Additionally, elucidating the comprehensive mechanisms of MSCs therapy in ALF remains equally important. With the ongoing advancement of MSCs clinical trials, it is anticipated that an increasing number of MSC-based therapeutic products will be developed and applied clinically in the future, offering new hope for patients suffering from conditions such as ALF.

In conclusion, to the best of our knowledge, the present study is the first to identify the hepcidin-ferroportin axis as a promising therapeutic target for ALF based on extensive functional experiments. Dysregulation of the hepcidin-ferroportin axis and the resulting iron metabolism disorder contribute to ferroptosis, thereby providing a more comprehensive understanding of ALF pathophysiology. Furthermore, Auranofin, an FDA-approved anti-rheumatic drug, has exhibited novel hepatoprotective properties by regulating iron metabolism and inhibiting ferroptosis through upregulation of hepcidin expression. More importantly, we have uncovered a novel mechanism by which MSCs can effectively regulate iron metabolism by activating the hepcidin-ferroportin axis via the PI3K/Akt/Nrf2 pathway. These findings may have substantial implications for the treatment strategies of ALF.

CRediT authorship contribution statement

Jinyong He: Writing – original draft, Visualization, Methodology, Investigation, Data curation. **Cong Du:** Writing – review & editing, Writing – original draft, Supervision, Investigation, Funding acquisition, Conceptualization. **Cuiping Li:** Software, Investigation. **Wei Li:** Software, Investigation. **Jinlan Qiu:** Software, Investigation. **Mingpeng Ma:** Software, Investigation. **Yunhao Chen:** Software, Methodology. **Qi Zhang:** Writing – review & editing, Supervision, Project administration, Funding acquisition, Conceptualization.

Financial support and sponsorship

This work is supported by grants from the National Nature Science Foundation of China (82170674, 82425010, 82300749, 82000620), Guangdong Basic and Applied Basic Research Foundation (2023A1515010583) and China Postdoctoral Science Foundation (2022M723610, 2024T171076).

Declaration of competing interest

The authors declare that they have no competing interests.

Appendix B. Supplementary data

Supplementary data to this article can be found online at https://doi.org/10.1016/j.redox.2025.103657.

Data availability

Data will be made available on request.

References

[1] R. Maiwall, A.V. Kulkarni, J.P. Arab, S. Piano, Acute liver failure, Lancet 404 (2024) 789–802.
[2] S. Tujios, R.T. Stravitz, W.M. Lee, Management of acute liver failure: update 2022, Semin. Liver Dis. 42 (2022) 362–378.
[3] V. Dong, V. Durkalski, W.M. Lee, C.J. Karvellas, et al., Outcomes of patients with acute liver failure not listed for liver transplantation: a cohort analysis, Hepatology Communications 8 (2024) e0575.
[4] C.J. Karvellas, T.M. Leventhal, J.L. Rakela, J. Zhang, V. Durkalski, K.R. Reddy, R. J. Fontana, et al., Outcomes of patients with acute liver failure listed for liver transplantation: a multicenter prospective cohort analysis, Liver Transpl 29 (2023) 318–330.
[5] X. Xu, K. Gong, L. Hong, X. Yu, H. Tu, Y. Lan, J. Yao, et al., The burden and predictors of 30-day unplanned readmission in patients with acute liver failure: a national representative database study, BMC Gastroenterol. 24 (2024) 153.
[6] H. Jaeschke, A. Ramachandran, Acetaminophen hepatotoxicity: paradigm for understanding mechanisms of drug-induced liver injury, Annu. Rev. Pathol. 19 (2024) 453–478.
[7] N. Gehrke, M.A. Wörns, A. Mann, N. Hövelmeyer, A. Waisman, B.K. Straub, P. R. Galle, et al., Hepatocyte Bcl-3 protects from death-receptor mediated apoptosis and subsequent acute liver failure, Cell Death Dis. 13 (2022) 510.
[8] S. Huang, Y. Wang, S. Xie, Y. Lai, C. Mo, T. Zeng, S. Kuang, et al., Hepatic TGFβr1 deficiency attenuates lipopolysaccharide/D-galactosamine-induced acute liver failure through inhibiting gsk3β-nrf2-mediated hepatocyte apoptosis and ferroptosis, Cell. Mol. Gastroenterol. Hepatol. 13 (2022) 1649–1672.
[9] D. Xie, S. Ouyang, The role and mechanisms of macrophage polarization and hepatocyte pyroptosis in acute liver failure, Front. Immunol. 14 (2023) 1279264.
[10] R.T. Stravitz, R.J. Fontana, C. Karvellas, V. Durkalski, B. McGuire, J.A. Rule, S. Tujios, et al., Future directions in acute liver failure, Hepatology 78 (2023) 1266–1289.
[11] Z.Y. Xing, C.J. Zhang, L.J. Liu, Targeting both ferroptosis and pyroptosis may represent potential therapies for acute liver failure, World J. Gastroenterol. 30 (2024) 3791–3798.
[12] B.R. Stockwell, Ferroptosis turns 10: emerging mechanisms, physiological functions, and therapeutic applications, Cell 185 (2022) 2401–2421.
[13] X. Jiang, B.R. Stockwell, M. Conrad, Ferroptosis: mechanisms, biology and role in disease, Nat. Rev. Mol. Cell Biol. 22 (2021) 266–282.
[14] C. Berndt, H. Alborzinia, V.S. Amen, S. Ayton, U. Barayeu, A. Bartelt, H. Bayir, et al., Ferroptosis in health and disease, Redox Biol. 75 (2024) 103211.
[15] J. Chen, X. Li, C. Ge, J. Min, F. Wang, The multifaceted role of ferroptosis in liver disease, Cell Death Differ. 29 (2022) 467–480.
[16] N. Yamada, T. Karasawa, H. Kimura, S. Watanabe, T. Komada, R. Kamata, A. Sampilvanjil, et al., Ferroptosis driven by radical oxidation of n-6

polyunsaturated fatty acids mediates acetaminophen-induced acute liver failure, Cell Death Dis. 11 (2020) 144.
[17] L. Mao, T. Zhao, Y. Song, L. Lin, X. Fan, B. Cui, H. Feng, et al., The emerging role of ferroptosis in non-cancer liver diseases: hype or increasing hope? Cell Death Dis. 11 (2020) 518.
[18] J. Wu, Y. Wang, R. Jiang, R. Xue, X. Yin, M. Wu, Q. Meng, Ferroptosis in liver disease: new insights into disease mechanisms, Cell Death Discov. 7 (2021) 276.
[19] C.Y. Wang, J.L. Babitt, Liver iron sensing and body iron homeostasis, Blood 133 (2019) 18–29.
[20] A.S. Vogt, T. Arsiwala, M. Mohsen, M. Vogel, V. Manolova, M.F. Bachmann, On iron metabolism and its regulation, Int. J. Mol. Sci. 22 (2021).
[21] I. Spivak, J. Arora, C. Meinzer, V. Durkalski-Mauldin, W.M. Lee, C. Trautwein, R. J. Fontana, et al., Low serum hepcidin is associated with reduced short-term survival in adults with acute liver failure, Hepatology 69 (2019) 2136–2149.
[22] K. Ferrao, N. Ali, K.J. Mehta, Iron and iron-related proteins in alcohol consumers: cellular and clinical aspects, J. Mol. Med. (Berl.) 100 (2022) 1673–1689.
[23] Y. Yu, L. Jiang, H. Wang, Z. Shen, Q. Cheng, P. Zhang, J. Wang, et al., Hepatic transferrin plays a role in systemic iron homeostasis and liver ferroptosis, Blood 136 (2020) 726–739.
[24] B. Angoro, M. Motshakeri, C. Hemmaway, D. Svirskis, M. Sharma, Non-transferrin bound iron, Clin. Chim. Acta 531 (2022) 157–167.
[25] E. Nemeth, T. Ganz, Hepcidin-ferroportin interaction controls systemic iron homeostasis, Int. J. Mol. Sci. 22 (2021).
[26] C.B. Billesbølle, C.M. Azumaya, R.C. Kretsch, A.S. Powers, S. Gonen, S. Schneider, T. Arvedson, et al., Structure of hepcidin-bound ferroportin reveals iron homeostatic mechanisms, Nature 586 (2020) 807–811.
[27] M. Kohjima, T. Yoshimoto, M. Enjoji, N. Fukushima, K. Fukuizumi, T. Nakamura, M. Kurokawa, et al., Hepcidin/ferroportin expression levels involve efficacy of pegylated-interferon plus ribavirin in hepatitis C virus-infected liver, World J. Gastroenterol. 21 (2015) 3291–3299.
[28] D. Vela, Low hepcidin in liver fibrosis and cirrhosis; a tale of progressive disorder and a case for a new biochemical marker, Mol Med 24 (2018) 5.
[29] H. Yang, J. Chen, J. Li, Isolation, culture, and delivery considerations for the use of mesenchymal stem cells in potential therapies for acute liver failure, Front. Immunol. 14 (2023) 1243220.
[30] S. Khan, S. Mahgoub, N. Fallatah, P.F. Lalor, P.N. Newsome, Liver disease and cell therapy: advances made and remaining challenges, Stem Cell. 41 (2023) 739–761.
[31] L. Chen, N. Zhang, Y. Huang, Q. Zhang, Y. Fang, J. Fu, Y. Yuan, et al., Multiple dimensions of using mesenchymal stem cells for treating liver diseases: from bench to beside, Stem Cell Rev Rep 19 (2023) 2192–2224.
[32] Y. Luan, X. Kong, Y. Feng, Mesenchymal stem cells therapy for acute liver failure: recent advances and future perspectives, Liver Research 5 (2021) 53–61.
[33] C. Hu, Z. Wu, L. Li, Mesenchymal stromal cells promote liver regeneration through regulation of immune cells, Int. J. Biol. Sci. 16 (2020) 893–903.
[34] A. Psaraki, L. Ntari, C. Karakostas, D. Korrou-Karava, M.G. Roubelakis, Extracellular vesicles derived from mesenchymal stem/stromal cells: the regenerative impact in liver diseases, Hepatology 75 (2022) 1590–1603.
[35] Y. Zhang, J. Zhang, H. Yi, J. Zheng, J. Cai, W. Chen, T. Lu, et al., A novel MSC-based immune induction strategy for ABO-incompatible liver transplantation: a phase I/II randomized, open-label, controlled trial, Stem Cell Res. Ther. 12 (2021) 244.
[36] Q. Liu, X. Chen, C. Liu, L. Pan, X. Kang, Y. Li, C. Du, et al., Mesenchymal stem cells alleviate experimental immune-mediated liver injury via chitinase 3-like protein 1-mediated T cell suppression, Cell Death Dis. 12 (2021) 240.
[37] S. Lin, H. Gao, H. Ma, Z. Liao, D. Zhang, J. Pan, Y. Zhu, A comprehensive meta-analysis of stem cell therapy for liver failure: assessing treatment efficacy and modality, Ann. Hepatol. 30 (2025) 101586.
[38] M. Shi, Y.Y. Li, R.N. Xu, F.P. Meng, S.J. Yu, J.L. Fu, J.H. Hu, et al., Mesenchymal stem cell therapy in decompensated liver cirrhosis: a long-term follow-up analysis of the randomized controlled clinical trial, Hepatol. Int. 15 (2021) 1431–1441.
[39] B.L. Lin, J.F. Chen, W.H. Qiu, K.W. Wang, D.Y. Xie, X.Y. Chen, Q.L. Liu, et al., Allogeneic bone marrow-derived mesenchymal stromal cells for hepatitis B virus-related acute-on-chronic liver failure: a randomized controlled trial, Hepatology 66 (2017) 209–219.
[40] M.L. Weiss, S. Medicetty, A.R. Bledsoe, R.S. Rachakatla, M. Choi, S. Merchav, Y. Luo, et al., Human umbilical cord matrix stem cells: preliminary characterization and effect of transplantation in a rodent model of Parkinson's disease, Stem Cell. 24 (2006) 781–792.
[41] S.L. Byrne, D. Krishnamurthy, M. Wessling-Resnick, Pharmacology of iron transport, Annu. Rev. Pharmacol. Toxicol. 53 (2013) 17–36.
[42] L. Jiang, J. Wang, K. Wang, H. Wang, Q. Wu, C. Yang, Y. Yu, et al., RNF217 regulates iron homeostasis through its E3 ubiquitin ligase activity by modulating ferroportin degradation, Blood 138 (2021) 689–705.
[43] L. Yang, H. Wang, X. Yang, Q. Wu, P. An, X. Jin, W. Liu, et al., Auranofin mitigates systemic iron overload and induces ferroptosis via distinct mechanisms, Signal Transduct. Targeted Ther. 5 (2020).
[44] D. Feng, X. Xiang, Y. Guan, A. Guillot, H. Lu, C. Chang, Y. He, et al., Monocyte-derived macrophages orchestrate multiple cell-type interactions to repair necrotic liver lesions in disease models, J. Clin. Investig. 133 (2023).
[45] J.P. Sikora, J. Karawani, J. Sobczak, Neutrophils and the systemic inflammatory response syndrome (SIRS), Int. J. Mol. Sci. 24 (2023).
[46] O. Krenkel, J.C. Mossanen, F. Tacke, Immune mechanisms in acetaminophen-induced acute liver failure, Hepatobiliary Surg. Nutr. 3 (2014) 331–343.
[47] M. Kremyanskaya, A.T. Kuykendall, N. Pemmaraju, E.K. Ritchie, J. Gotlib, A. Gerds, J. Palmer, et al., Rusfertide, a hepcidin mimetic, for control of erythrocytosis in polycythemia vera, N. Engl. J. Med. 390 (2024) 723–735.
[48] E. Zhao, R. Liang, P. Li, D. Lu, S. Chen, W. Tan, Y. Qin, et al., Mesenchymal stromal cells alleviate APAP-induced liver injury via extracellular vesicle-mediated regulation of the miR-186-5p/CXCL1 axis, Stem Cell Res. Ther. 15 (2024) 392.
[49] L. Pan, C. Liu, Q. Liu, Y. Li, C. Du, X. Kang, S. Dong, et al., Human Wharton's jelly-derived mesenchymal stem cells alleviate concanavalin A-induced fulminant hepatitis by repressing NF-κB signaling and glycolysis, Stem Cell Res. Ther. 12 (2021) 496.
[50] P.J. Lim, T.L. Duarte, J. Arezes, D. Garcia-Santos, A. Hamdi, S.R. Pasricha, A. E. Armitage, et al., Nrf2 controls iron homeostasis in haemochromatosis and thalassaemia via Bmp6 and hepcidin, Nat. Metab. 1 (2019) 519–531.
[51] B. Galy, M. Conrad, M. Muckenthaler, Mechanisms controlling cellular and systemic iron homeostasis, Nat. Rev. Mol. Cell Biol. 25 (2024) 133–155.
[52] R. Yan, B. Lin, W. Jin, L. Tang, S. Hu, R. Cai, NRF2, a superstar of ferroptosis, Antioxidants 12 (2023).
[53] F. Lin, W. Chen, J. Zhou, J. Zhu, Q. Yao, B. Feng, X. Feng, et al., Mesenchymal stem cells protect against ferroptosis via exosome-mediated stabilization of SLC7A11 in acute liver injury, Cell Death Dis. 13 (2022) 271.
[54] M.J. Wang, H.L. Zhang, F. Chen, X.J. Guo, Q.G. Liu, J. Hou, The double-edged effects of IL-6 in liver regeneration, aging, inflammation, and diseases, Exp. Hematol. Oncol. 13 (2024) 62.
[55] D. Jovic, Y. Yu, D. Wang, K. Wang, H. Li, F. Xu, C. Liu, et al., A brief overview of global trends in MSC-based cell therapy, Stem Cell Rev Rep 18 (2022) 1525–1545.